Available online at www.sciencedirect.com
SCIENCE DIRECT®
International Journal of Mass Spectrometry 228 (2003) 373–388
International Journal of Mass Spectrometry
www.elsevier.com/locate/ijms

Distinguishing the topology of macrocyclic compounds and catenanes

Christoph A. Schalley[a,*], Joerg Hoernschemeyer[a], Xiyou Li[a,1], Gabriele Silva[a], Patrick Weis[b,2]

[a] *Kekulé-Institut für Organische Chemie und Biochemie der Universität, Gerhard-Domagk-Str. 1, D-53121 Bonn, Germany*
[b] *Institut für Physikalische Chemie der Universität, Kaiserstr. 12, D-76128 Karlsruhe, Germany*

Received 12 November 2002; accepted 18 March 2003

Dedicated to Helmut Schwarz, a great scientist and teacher, on the occasion of his 60th birthday.

Abstract

The paper explores different possibilities to distinguish macrocyclic oligolactam species with different molecular topologies by ESI mass spectrometry. Collision-induced fragmentation provides unambiguous fragmentation patterns: Monocyclic rings upon single and double protonation predominantly lose water molecules, while catenanes, i.e., two chain-like interlocked macrocycles, undergo ring cleavage followed by loss of a whole ring. At higher collision energies and under multiple collision conditions, a series of different fragments is observed which can be categorized into six different types. These fragments are structure indicative and provide evidence for the connectivities of building blocks within the macrocycles. Gas-phase ion mobility experiments on the other hand result in a good agreement between experimental collision cross-sections and structure predictions from theory. This method does not provide unequivocal differences between monocyclic rings and catenanes due to almost identical cross-sections, but it provides a tool to distinguish between knots (twisted monocyclic rings) and (untwisted) rings.

Keywords: Supramolecular chemistry; Macrocycles; Catenanes; Knots; Mass spectrometry; Ion mobility experiments

1. Introduction

Diamine **1** and analogous compounds with appropriate substituents can be converted in one reaction step into tetralactam macrocycles such as **2**–**6** (Scheme 1) by simple amide bond formation with the corresponding isophthalic acid dichloride [1–3]. Although this reaction is carried out under dilution conditions to promote formation of macrocyclic products, usually the generation of side products is observed, among them those with two and three times higher mass. In principle, different topologies can be imagined for these compounds. Those with twice the molecular mass may correspond to catenanes [4–8] such as **7**–**10** or to octalactam macrocycles such as **11**. One of the most spectacular products of such a cyclization experiment of **1** with 2,6-pyridine dicarboxylic

* Corresponding author. Tel.: +49-22873-5784; fax: +49-22873-5662.
E-mail addresses: c.schalley@uni-bonn.de (C.A. Schalley), patrick.weis@chemie.uni.karlsruhe.de (P. Weis).
[1] Present address: Department of Chemistry, Shandong Normal University, Ji Nan 250014, China.
[2] Co-corresponding author.

1387-3806/$ – see front matter © 2003 Elsevier Science B.V. All rights reserved.
doi:10.1016/S1387-3806(03)00131-3

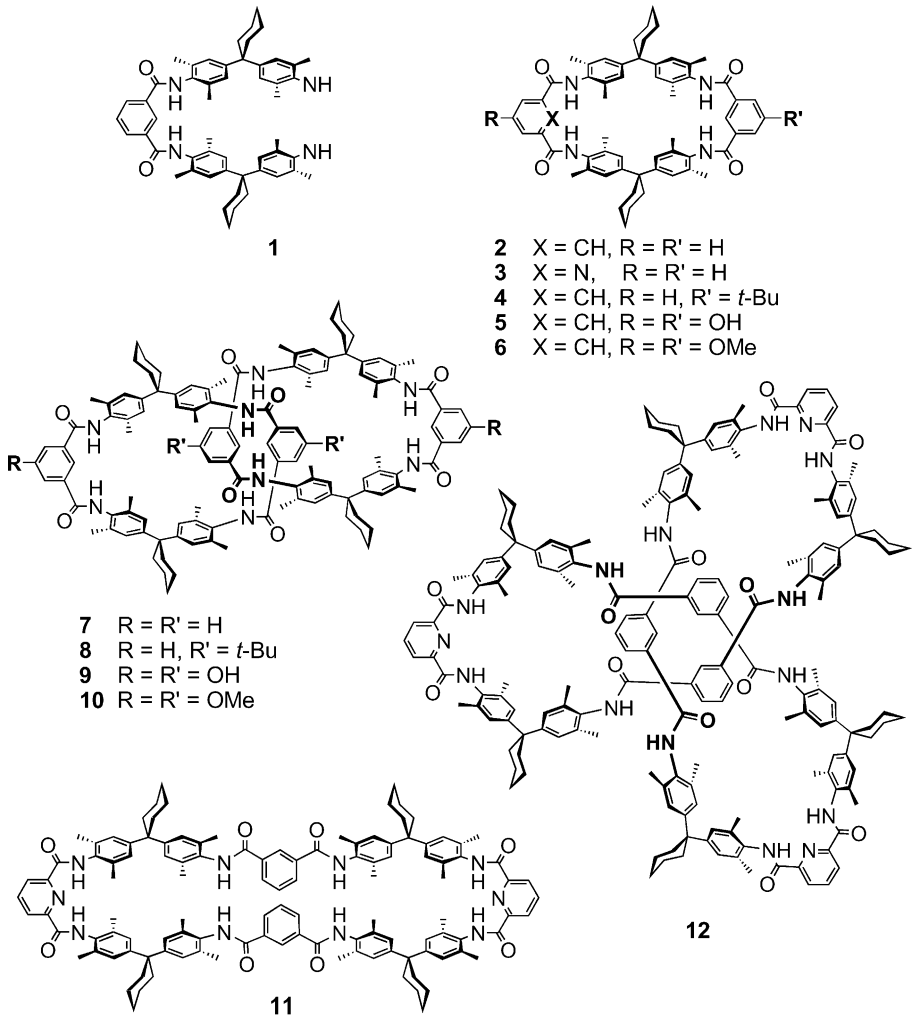

Scheme 1.

acid dichloride is the trefoil molecular knot **12**, which was recently discovered by Vögtle and co-workers [9,10]. Both catenanes and knots form due to template effects mediated by hydrogen bonding [5]. NMR spectrometry is of limited value for the characterization of these species, since they all contain identical building blocks. For intertwined molecules such as the catenanes, small upfield shifts of the signals for the molecule's parts which are mutually positioned in the cavity of the other wheel are often observed and are caused by the anisotropy of the aromatic rings in their neighborhood. However, these shifts can only be unambiguously interpreted, when the corresponding octalactam macrocycle is also formed and then serves for comparison [11]. However, often only one of the two topologies is realized. For example, diamine **1** gives the catenane **2** when reacted with isophthalic acid dichloride, while no octalactam macrocycle could be isolated. Vice versa, its reaction with 2,6-pyridine dicarboxylic acid dichloride only yields macrocycle **11**. In these cases, the exact analysis by NMR experiments is difficult and often suffers

from significant uncertainties. Consequently, it would be extremely helpful to devise a practical analytical procedure for an unambiguous distinction of the two topologies.

Although a powerful means for the examination of supramolecular complexes [12,13], mass spectrometry at first sight does not seem to be suitable to solve this problem, because a catenane and its corresponding octalactam macrocycle have the same elemental composition, and thus are isobaric. Nevertheless, there are different experiments which in principle may provide the necessary information: (i) ion mobility experiments [14] provide collisional cross-section data which can be compared with cross-sections calculated from energy-favored conformations obtained by molecular modeling. One might expect a catenane to be more compact than the octalactam macrocycle because of its intertwined topology, (ii) tandem-MS experiments could result in different structure-indicative fragmentations, and (iii) even if the fragmentations are similar for both species, there might be a difference between the collision-energy onsets. If, for example, one of the wheels of a catenane is opened upon protonation, the second wheel easily would deslip, while for a similar reaction of the analogous octalactam macrocycle two covalent bonds must be cleaved, a process which would demand a higher collision energy. In this contribution, we explore these possibilities and find that the most convenient procedure is the collision-induced fragmentation in an MS/MS experiment which leads to completely different fragmentation patterns.

2. Experimental

2.1. Syntheses

The syntheses, the purification, and the characterization of all compounds used in this study have been described before [1–3,9,15,16]. The N-deuterated macrocycle **4**-d_4 was prepared by stirring **4** in deuterated methanol/dichloromethane 9:1 for 48 h. A ^{1}H-NMR spectrum confirms the exchange of all amide protons against deuterium (>96% of all NH protons exchanged).

2.2. Tandem mass spectrometric experiments

ESI mass spectra and MS/MS spectra were recorded on a Micromass Q-TOF 2 mass spectrometer equipped with a nanospray ion source with Z geometry. Typically, methanol (deuterated methanol for **4**-d_4) served as the spray solvent and 50 μM solutions of the analytes were used. When solubility in methanol was too low, an as small as possible amount of dichloromethane was added. Some samples predominantly yielded sodium adducts. In these cases, the signal for the protonated species can be increased in intensity by addition of ca. 1% of formic acid to the sample solution. Typical capillary voltages were 900–1200 V, the cone voltage was optimized within the range of 50–90 V for maximum intensity of the desired ion subjected to the MS/MS experiments. The whole range of isotopic ions of interest was isolated and admitted to the collision cell which was operated with Ar gas at a pressure of 0.5 mbar in order to provoke collisional activation. The acceleration voltage was increased step by step in order to monitor the fragmentation behavior at different collision energies. Spectra were recorded by averaging 15–50 scans for an improved signal-to-noise ratio.

2.3. Ion mobility experiments

The gas phase ion mobility technique is a fairly direct way to obtain structural information, since it is directly connected to the collision cross-section of the molecule. This method involves the determination of the time it takes for an ion to drift through a gas-filled cell guided by a static electrical field. The method as such has been developed long ago by McDaniel and Mason [14], the combination with modern mass spectrometry has been pioneered by the Bowers group [17] and has been used by several groups to determine the conformations of, for example, polymers [18], peptides [19–21], and—very recently—amino acid clusters such as the serine octamer [22,23].

The ion collision cross-section measurements presented here were performed in an instrument that comprises a combination of an electrospray ion source, a time-of-flight mass spectrometer, an ion mobility drift cell, and a quadrupole mass filter. Details of the experimental setup have been described elsewhere [24]. Briefly, the samples were dissolved in a 50/50/1 mixture of methanol, dichloromethane and acetic acid, electrosprayed and mass selected in a time-of-flight mass spectrometer. The mass selected ion beam was injected into the drift cell (110 mm long, 0.5 mm entrance and exit orifices, filled with 5–10 mbar helium buffer gas at 300 K). The injected ion packet was guided through the buffer gas in the cell under the influence of a weak electric field (typically 10 V/cm). After leaving the cell, the ions passed through the quadrupole mass filter (for rejection of possible fragmentation products) and are detected by means of a channeltron electron multiplier. The drift time distributions were acquired as a function of the applied drift voltage, and from the plot of the arrival time (distribution maximum) against drift voltage we obtained the ion mobility and finally the collision cross-section—which can be directly compared with predictions from theory.

2.4. Molecular modeling: cross-section calculations

For relatively floppy molecules like these macrocycles, it is almost impossible to find the global minimum. On the other hand, this is not necessary for comparison with the ion mobility measurements since the experiment itself reflects a thermal average of different conformers. The method of choice is therefore to run molecular dynamics simulations and get an averaged cross-section for a large number of possible conformations. We used the AMBER force field [25–27] implemented in the HyperChem 6 package [28]. We used a simulated temperature of 1000 K with a time step of 1 fs. After annealing for 5 ps (5000 steps) we cooled down to room temperature over a time interval of another 5 ps. Then the simulation was stopped and the resulting geometry optimized. This procedure was repeated for total a time interval of 1 ns, i.e., 100 sample conformers were taken. For these structures, we calculated the collision cross-section with two different methods: the projection approximation [29] which represents a lower boundary to the experimental value and the exact hard spheres scattering model [30] which usually represents an upper boundary. For comparison with experiment we took the average of both methods and of the 100 conformers.

3. Results and discussion

3.1. ESI mass spectra

Nanospray ionization of methanol solutions of the compounds shown in Scheme 1 results in mass spectra which typically contain the protonated and sodiated pseudo-molecular ions. In addition, doubly charged species are usually observed. A representative example is shown in Fig. 1. This spectrum of catenane **7** exhibits the protonated complex **7**•H^+ at *m*/*z* 1810 accompanied by its sodium derivative **7**•Na^+ at *m*/*z* 1832 and three doubly charged ions at *m*/*z* 905, 916, and 927 which correspond to the catenane ionized by two protons, one proton plus one sodium ion, and two sodium ions. Some minor fragments are seen at lower *m*/*z* ratios. The relative amount of singly and doubly charged ions changes depending on the structure of the compound. Typically, the tetralactam macrocycles **2**–**6** yield only low abundances of doubly protonated species, while they are more prominent for the larger macrocycles and catenanes. For some of the compounds, the intensities of proton adducts had to be increased relative to that of the sodium adduct by addition of a small amount of formic acid in order to generate intensities sufficient for MS/MS experiments (Scheme 2).

Recently, a macrocyclization intended to produce macrocycle **13** with its biquinoline metal coordination site resulted in two side products: Octalactam macrocycle **14** (32% yield) and catenane **15** (1% yield) [11]. These two species can easily and reliably be distinguished by ^{1}H-NMR spectroscopy, because the chemical shift of the biquinoline 3,3′ protons is very sensitive

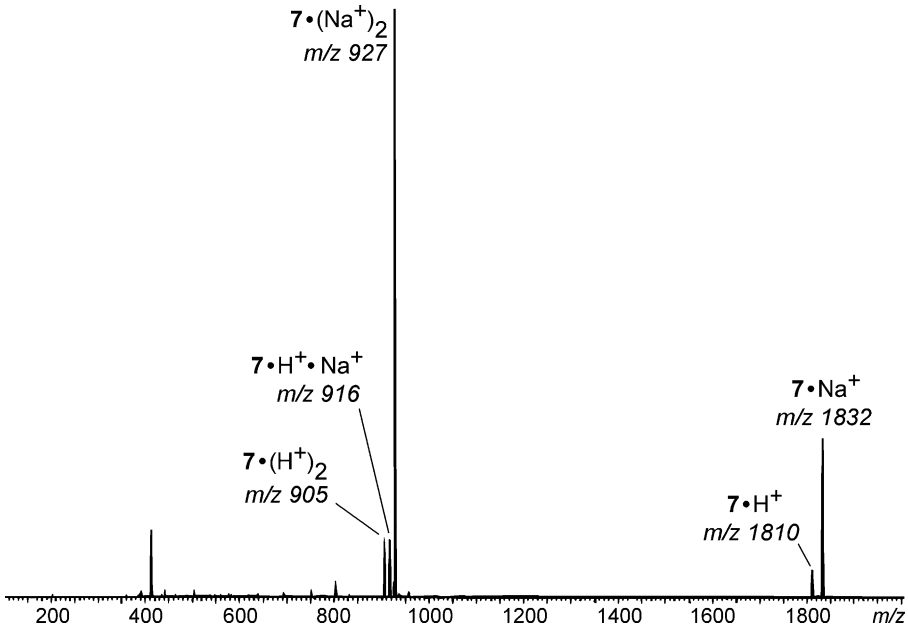

Fig. 1. Nanospray mass spectrum of a 50 μM solution of catenane **7** in methanol with ca. 1% formic acid added.

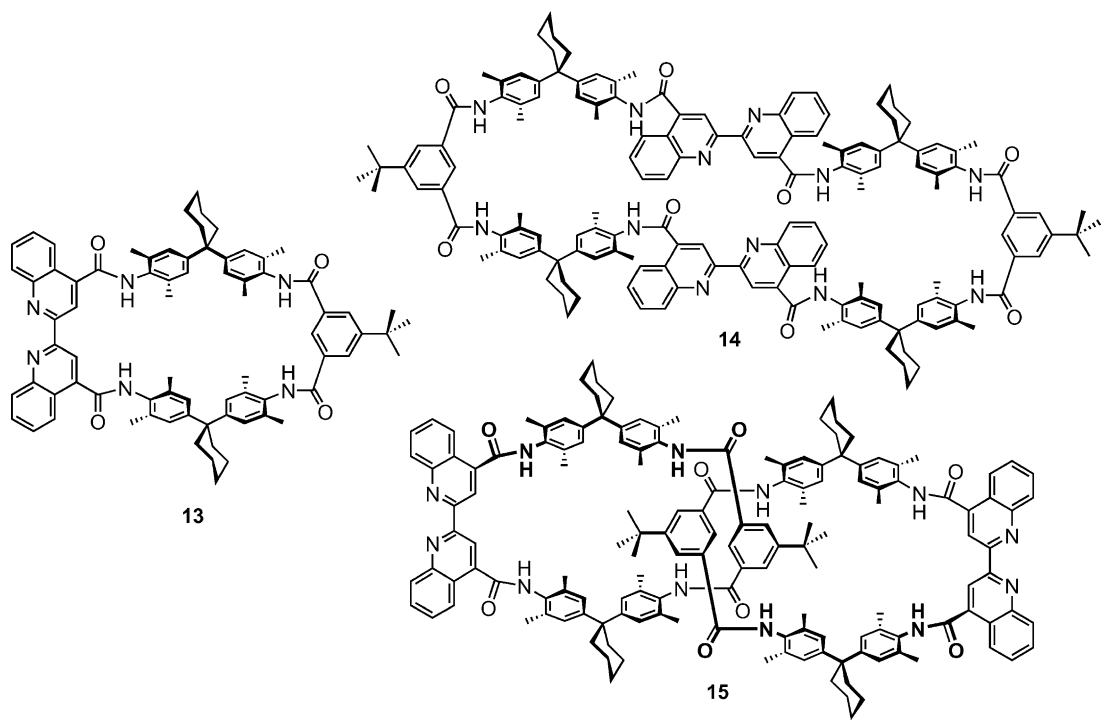

Scheme 2.

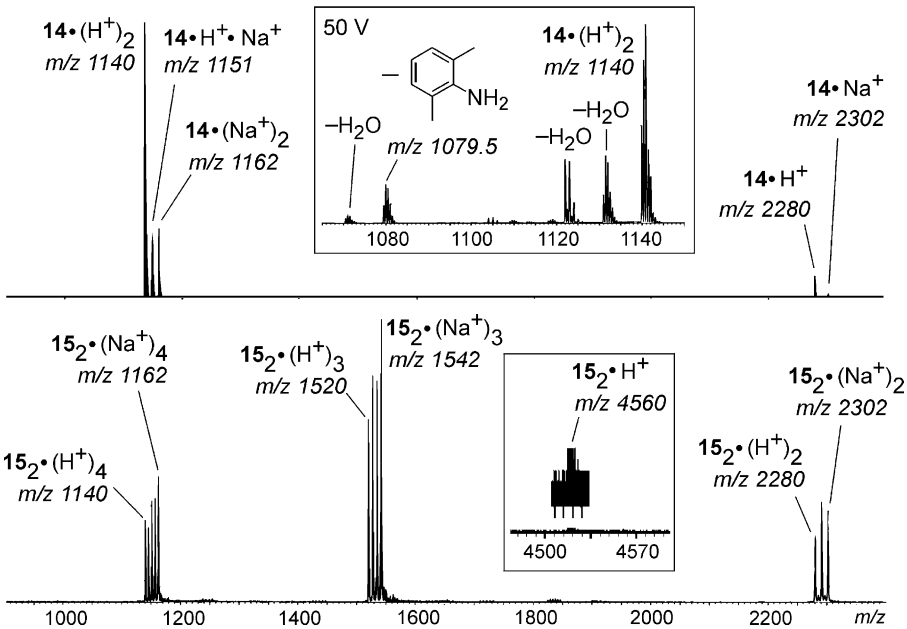

Fig. 2. Nanospray mass spectra of 50 μM solutions of octalactam macrocycle **14** (top) and catenane **15** (bottom) in methanol. The signals in the bottom spectrum which are not labeled correspond to complexes ionized by mixtures of protons and sodium ions and appear equally spaced within each group at mass differences of $\Delta m = 5.5$, 7.3, and 11.0 amu (from left to right) as expected for quadruply, triply, and doubly charged dimers $\mathbf{15}_2$, respectively. The inset in the bottom spectrum shows the signal for the proton-bridged dimer $\mathbf{15}_2\bullet H^+$. The top inset shows part of the MS/MS spectrum of doubly protonated $\mathbf{14}(H^+)_2$ after collisions with argon at an acceleration voltage of 50 V.

to the conformation of the biquinoline unit. Consequently, two topologically different species with the same elemental composition could directly be compared by mass spectrometry. Macrocycles **13** and **14** yield mass spectra analogous to those of **2** and **11**, respectively. As an example, the spectrum obtained with **14** is shown in Fig. 2 (upper panel). Rather prominent signals for doubly charged ions are observed around *m*/*z* 1150 (Fig. 2) accompanied by the protonated and sodiated monocations at *m*/*z* 2280 ($\mathbf{14}\bullet H^+$) and 2302 ($\mathbf{14}\bullet Na^+$). However, to our surprise the corresponding catenane **15** behaved quite differently. Three sets of signals are found (Fig. 2, bottom) centered around *m*/*z* 1150 (5 signals), *m*/*z* 1530 (4 signals) and *m*/*z* 2290 (3 signals). In all of these clusters, the signals are evenly spaced indicating that they correspond to quadruply, triply, and doubly charged dimers of the catenane ionized either by protons, sodium ions or all possible combinations of these. The charge states are confirmed by isotope pattern analysis as well as the spacing between the signals. Consequently, the catenane differs from the octalactam macrocycle in that it almost exclusively forms dimeric ions $\mathbf{15}_2(H^+)_m(Na^+)_n$ (i.e., these ions built from two complete catenanes thus containing a total of four of the smaller tetralactam macrocycles) upon nanospray ionization ($m = 0$–4, $n = 0$–4 with $m + n = 2$–4). No singly charged ion $\mathbf{15}\bullet H^+$ is found within the isotope pattern of $\mathbf{15}_2(H^+)_2$. Also, the intensities of the signals for the proton or sodium bridged dimers $\mathbf{15}_2\bullet H^+$ and $\mathbf{15}_2\bullet Na^+$ hardly exceed the signal to noise ratio (bottom inset in Fig. 2).

This strong tendency of the catenane to form dimeric species can be understood, if one assumes protonation at the biquinoline moieties. While the octalactam macrocycle according to modeling is capable of bridging both biquinoline sites by a proton intramolecularly, the catenane cannot. Thus, double protonation occurs making the formation of dimers

possible by a twofold proton bridge between the two monomers. This explanation is also in line with the low intensity of the signal for $\mathbf{15}_2\bullet H^+$, where the second proton is missing and only one proton bridge can be formed. For the corresponding Cu(I) complexes very similar results have been found [11]. Although **15** is a special case, since the biquinoline units are needed for this effect, it is a remarkable difference in behavior which is only caused by the topology of the molecules, which otherwise have the same building blocks, the same elemental composition, and—at least roughly—the same size.

3.2. Tandem-MS experiments

As the next step, the fragmentation behavior was examined by MS/MS experiments (Fig. 3). Let us start with a discussion of the collision-induced fragmentations of protonated macrocycle $\mathbf{2}\bullet H^+$ (*m/z* 905), which was studied at different acceleration voltages, i.e., different average collision energies. At a low voltage of 30 V, a single fragment is observed which corresponds to the loss of a water molecule (*m/z* 887). With increasing collision energies, this fragment appears with rapidly growing abundances, while the intensity

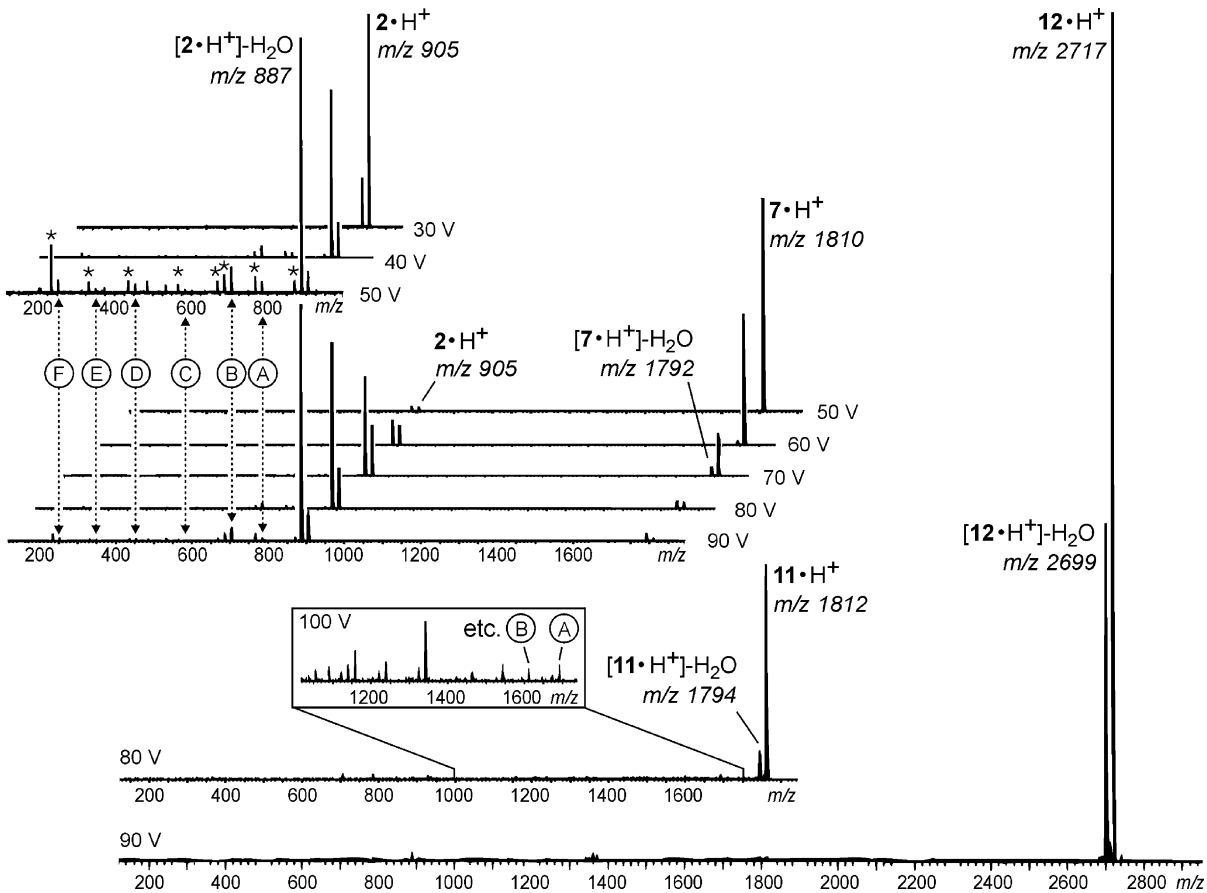

Fig. 3. MS/MS spectra (from top to bottom) of tetralactam macrocycle **2**, catenane **7**, octalactam macrocycle **11**, and the trefoil knot **12**. All sample solutions were 50 μM in methanol/dichloromethane mixtures. Each spectrum is labeled with the acceleration voltage and printed on the same scale in order to facilitate comparison. For **2** and **7**, several spectra are shown which were recorded at different collision energies, but otherwise identical experimental conditions. Clearly, at higher collision energies, a series of fragmentations occurs which are indicated with letters according to Scheme 3. Asterisks indicate water losses from the next larger species. The inset in the MS/MS spectrum of **11** depicts fragmentations occurring at acceleration voltages of 100 V which proceed in close analogy to those of $\mathbf{2}\bullet H^+$.

of the signal corresponding to the parent ion decreases significantly and almost completely vanishes at voltages around 60 V. Several other fragmentations occur and appear in the spectra with much lower intensities. These fragmentations can be summed up into six categories (A)–(F) as indicated in Fig. 3. All these fragments can be assigned to two subsequent bond cleavages within the macrocycle and loss of the neutral fragment and as we will discuss below, there is evidence that the first step is cleavage of the protonated amide bond (Scheme 3). Since it is not straightforward to determine from these spectra whether the decomposition processes are all direct or consecutive processes, they are shown in Scheme 3 as *formal* fragments that would require a minimal amount of rearrangement. Basically, these fragments confirm the connectivities between the different subunits from which the macrocycle is built. Interestingly, some of these decomposition reactions involve the cleavage of one of the C–C bonds at the spiro centers (pathways A, B, E, and F). This bond might be favored over other possibilities due to the intermediate formation of benzylic radicals (or cations).

Two experiments were performed in order to gather somewhat more detailed information on these fragmentations. When an unsymmetrical macrocycle such as the *t*-butyl substituted tetralactam wheel **4** is subjected to the same experiments, all signals that retain only one of the isophthalic acid building blocks are expected to split into two signals with a mass difference of $\Delta m = 56$. All fragments which do not lose this subunit should appear at positions

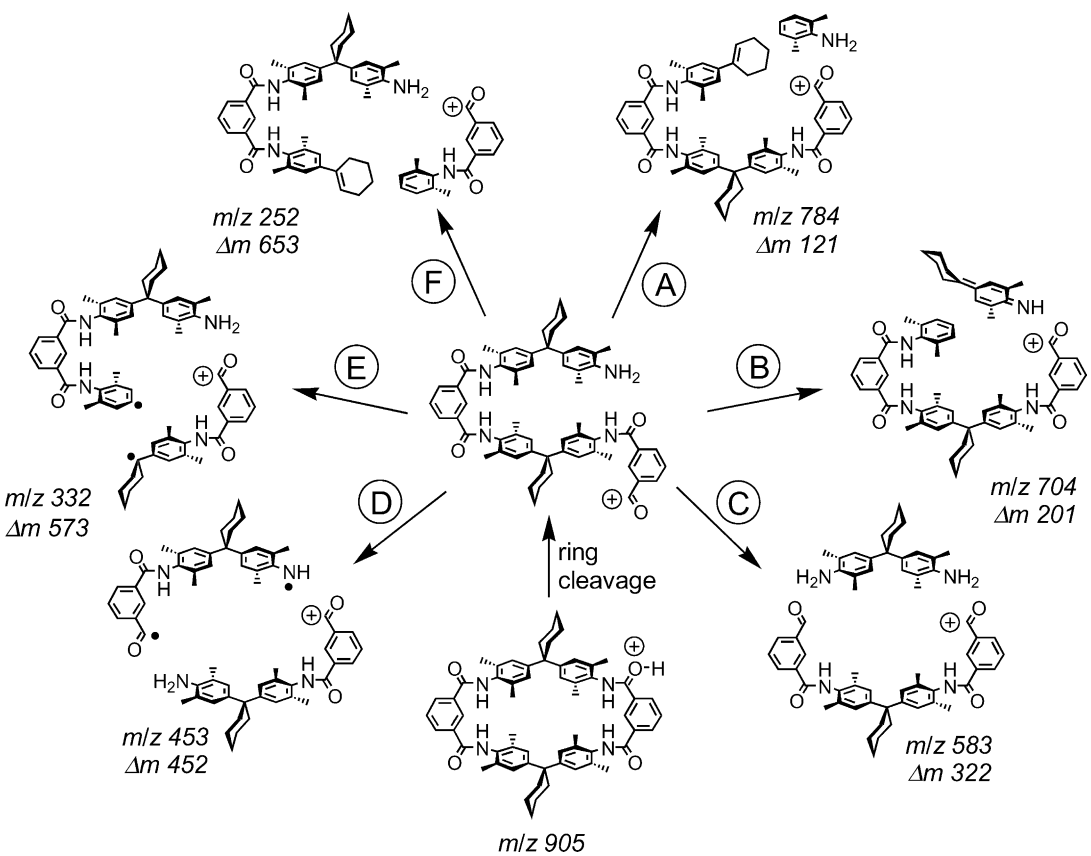

Scheme 3.

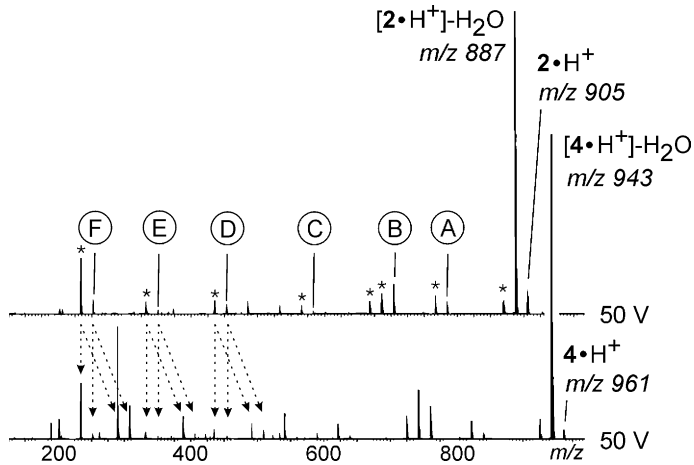

Fig. 4. Comparison of collision-induced decompositions of tetralactam wheels **2** and **4** at an acceleration voltage of 50 V. Fragments are indicated as given in Fig. 3. Note that **4** is unsymmetrically substituted with a *t*-butyl group. This doubles the signals for fragments in which only one of the isophthalic acid building blocks is retained (arrows).

shifted to higher masses by the same distance. Finally, all ions which have lost both isophthalic acid units should remain at the position where they also appear in the spectrum of **2**. This is indeed observed (Fig. 4) and the findings are in agreement with the fragmentations postulated in Scheme 3. The second experiment aimed at distinguishing the origin of hydrogen atoms involved in the water loss (and also in the other decomposition reactions). Macrocycle **4** was stirred in deuterated methanol/dichloromethane 9:1 for 2 days. ^{1}H-NMR spectroscopy confirmed a complete exchange (>96%) of the amide protons against deuterium. Upon nanospray ionization from a deuterated methanol solution, **4**-d_4•D$^+$ (*m*/*z* 966) was formed and used for the same series of collision experiments (Fig. 5). As expected, the loss of D_2O ($\Delta m = 20$ amu) is predominant in the 30 V MS/MS spectrum. A plausible mechanism, how D_2O could be formed from **4**-d_4•D$^+$ is shown in Scheme 4. At higher collision energies, however, the isotopic peak at *m*/*z* 947 corresponding to the loss of HDO increases relative to that at *m*/*z* 946 which is due to the

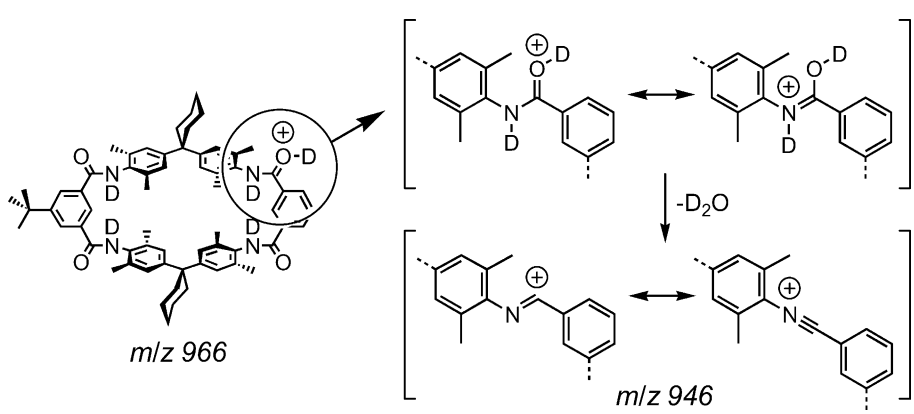

Scheme 4.

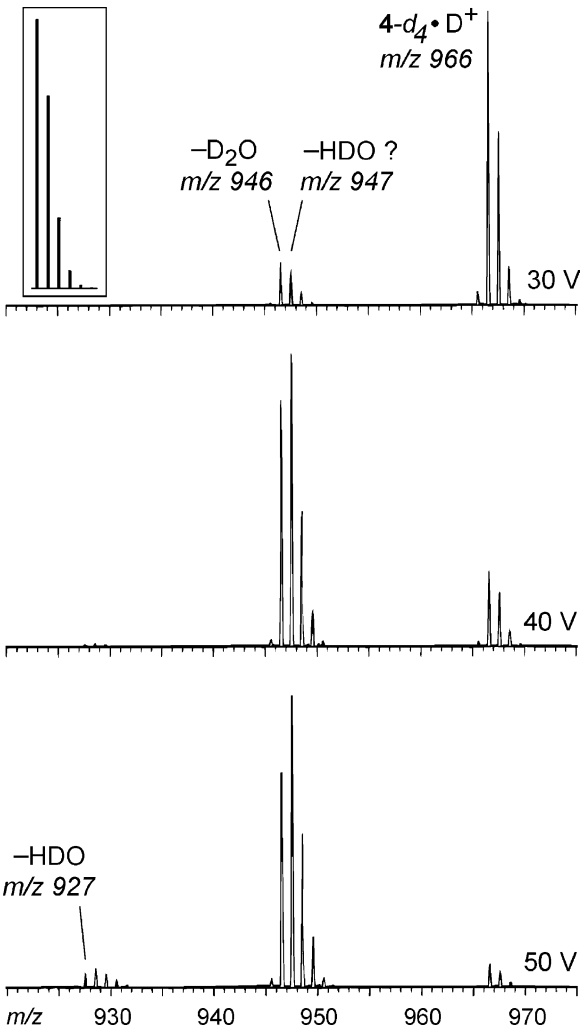

Fig. 5. Water loss region of the MS/MS mass spectra of **4**-d_4 (macrocycle **4** with all amide protons exchanged against deuterium) at different collision energies. The isotope pattern of the signal for the D_2O/HDO loss from **4**-d_4•H^+ changes with increasing collision energy towards increasing contributions of HDO expulsion, and thus indicates a partial H/D scrambling. The inset shows the isotope pattern calculated on the basis of natural abundances.

expulsion of D_2O. Since similar effects are observed for the other fragments, we attribute this finding to a partial intramolecular exchange between the amide N–D deuterons and the methyl C–H hydrogen atoms which experience some activation due to the benzylic positions. This process becomes more prominent at higher collision energies, and thus is likely more energy demanding than the expulsion of D_2O. Nevertheless, it unfortunately limits the amount of information which can be obtained from the deuteration experiment.

Before discussing the fragmentation pattern of the other macrocycles and catenanes, it should be noted that all fragments formed as indicated in Scheme 3 are accompanied by consecutive water losses (asterisks in Fig. 3). In the MS/MS spectra of **4**-d_4•D^+, they all appear at distances of $\Delta m = 19$ amu relative to the next higher signal. This indicates that only the first water loss corresponds to D_2O, while all subsequent water expulsions are due to the liberation of HDO. This also applies to the second water loss observed in the 50 V MS/MS spectrum of **4**-d_4•D^+ (Fig. 5, bottom). Since no consecutive D_2O losses are observed, it can be concluded that all water losses except the first one involve a C–H hydrogen atom. Again, due to the benzylic position, we favor the methyl C–H atoms as the source for them. For the time being, we however, cannot give final evidence for this assumption.

Following this detailed discussion of the fragmentation processes of the tetralactam macrocycles **2** and **4**, we can discuss the fragmentation behavior of the other species more rapidly. Catenane **7** and octalactam macrocycle **11** differ from each other in two significant respects. While **11**•H^+ (*m*/*z* 1812) predominantly loses a water molecule in close analogy to **2**•H^+, the protonated catenane yields only a very minor signal for such a reaction. Instead, a stronger signal is observed at *m*/*z* 905 which corresponds to **2**•H^+ or rather its open-chain analogue. This fragment can easily be explained by a ring cleavage reaction within one of the two macrocycles, which is then followed by deslipping of the second macrocycle finally leaving the complex. At higher collision energies, this fragment undergoes the same fragmentations that were observed from macrocycle **2**•H^+. As mentioned above, this is in line with the assumption that **2**•H^+ also undergoes ring cleavage at one of the amide bonds, and thus generates a structurally equivalent cation. These results then indicate that ring opening reactions are quite facile and likely compete with the water loss. The second difference between catenane and octalactam

macrocycle is the absence of fragments between *m/z* 905 and 1790 in the catenane spectrum even at higher collision energies. The octalactam macrocycle reveals fragments in this region similar to those observed for the tetralactam macrocycles **2** and **4** (inset in Fig. 3). Briefly, this means that the catenane undergoes deslipping of one of the two wheels, while other fragmentations would require higher energies, and thus do not occur. Macrocycle **11**•H^+, instead, forms fragments throughout the whole mass range between *m/z* 200 and 1800, because there is no such low energy pathway when after the ring opening step all parts of the molecule are still covalently connected. Finally, it should be noted that the trefoil knot is a monocyclic macrocycle, although it is mechanically intertwined. Consequently, it behaves in exact analogy to the other macrocycles and reveals a water loss upon collisional activation in an MS/MS experiment.

The acceleration voltages with which the ions enter the collision cell of course do not correspond to exact collision energies. However, on average the collision energy is higher at higher voltages. It is not unexpected that catenane **7**•H^+ and the octalactam macrocycle **11**•H^+ fragment at somewhat higher collision energies than the small macrocycle **2**•H^+. This can be explained by invoking the different molecule sizes, which allow to store more vibrational energy within the larger molecules before the threshold for fragmentation is reached. It is however in support of the analysis given above that **11**•H^+ fragments only to a minor extent at a voltage of 80 V, while the parent ion of catenane **7** is already almost completely destroyed at the same collision energy.

As a last remark, let us comment on doubly protonated species. Octalactam macrocycle **14**$(H^+)_2$ (*m/z* 1140) may serve as an example. According to the results presented so far, one would expect that fragments are formed indicative of the octalactam wheel structure. The top inset in Fig. 2 confirms this expectation: At an acceleration voltage of 50 V, two consecutive water losses are observed and signals for other fragments are found in the spectrum. Clearly visible, a doubly charged ion is generated which corresponds to the loss of a neutral dimethylaniline fragment, i.e., a type (A) fragmentation according to the classification in Scheme 3. It should be noted that lower acceleration voltages are needed for the fragmentation of doubly as compared to singly charged species, because the kinetic energy of the ions is proportional not only to the acceleration voltage, but also to the number of charges. Consequently, doubly protonated macrocycle **14**•H^+ confirms exactly the findings for singly charged particles.

3.3. Ion mobility experiments

Fig. 6a shows as an example the arrival time distribution of protonated catenane **8**•H^+, with a molar weight of 1923.5 amu. This mass/charge ratio was selected in the TOF and injected into the drift cell, the quadrupole mass filter after the cell has been set to RF-only mode, i.e., it acts as a high pass filter. The

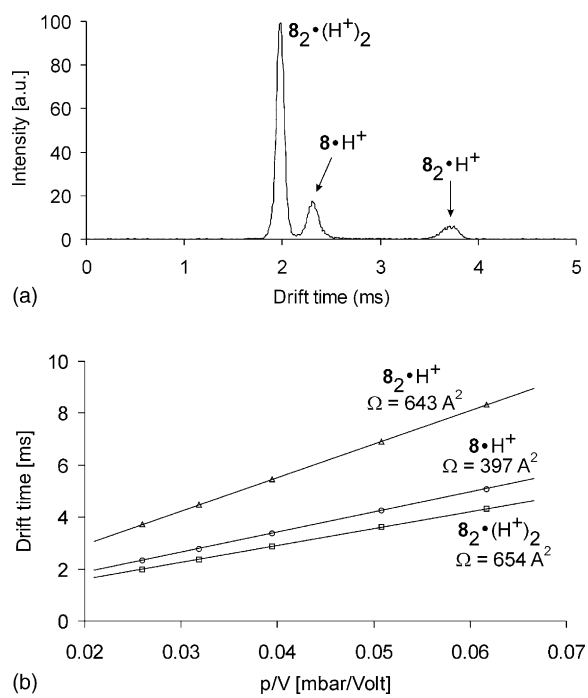

Fig. 6. (a) Drift time distribution of catenane **8** at a helium buffer gas pressure of 7.69 mbar, a temperature of 299 K, and a drift voltage of 296 V. (b) Maxima of the drift time distributions vs. ratio of helium pressure and applied drift voltage. The slopes of the plots are directly proportional to the collision cross-sections.

arrival time distribution showed three different peaks, the first one corresponding to the doubly charged dimeric ion $\mathbf{8}_2(H^+)_2$, the second to the singly charged catenane $\mathbf{8}\bullet H^+$ and the third peak to the singly charged dimer which was formed upon injection into the drift cell. This could be confirmed by a control experiment: By setting the quadrupole mass filter to high resolution, the third peak disappears since it corresponds to twice the mass of catenane **8**. By variation of the voltage across the cell (while keeping the helium pressure and temperature constant) and measuring the maxima of arrival time distribution as a function of the voltage/pressure ratio we obtain a straight line (see Fig. 6b). From the slope of this line we can directly obtain the collision cross-section, cf. [24].

Analogously, the cross-sections for the protonated macrocycles **2**–**12** as given in Table 1 were determined. The experimental errors are in the order of 3%. These cross-sections can be compared with the theoretical values obtained by averaging over 100 conformers from a molecular dynamics simulation (see above).

As can be seen from Table 1, the agreement between theoretical and experimental values is usually better than 3%, i.e., these structures could be confirmed by the ion mobility measurement. For the $\mathbf{11}\bullet H^+$ the difference is 5%, i.e., at the confidence limit, but this is most likely due to unusually large conformers sampled in the modeling (see below). The monomeric units $\mathbf{2}\bullet H^+$, $\mathbf{3}\bullet H^+$, $\mathbf{4}\bullet H^+$, and $\mathbf{6}\bullet H^+$ had cross-sections between 225 and 249 Å^2, depending on substitution. The catenanes $\mathbf{7}\bullet H^+$, $\mathbf{8}\bullet H^+$, and $\mathbf{10}\bullet H^+$ had experimental cross-sections between 371 and 397 Å^2, in agreement with theory. The monocyclic macrocycle $\mathbf{11}\bullet H^+$ represents essentially an isomer of the catenane $\mathbf{7}\bullet H^+$ (only two benzene rings are replaced by pyridine rings). Since $\mathbf{11}\bullet H^+$ is topologically much less constrained we expected it to have a more open structure, and thus a significantly larger cross-section than the catenane $\mathbf{7}\bullet H^+$. Surprisingly, the experimental cross-section of $\mathbf{11}\bullet H^+$ (362 Å^2) agreed within the experimental errors with the cross-section of $\mathbf{7}\bullet H^+$ (371 Å^2). This finding was essentially confirmed by the molecular dynamics simulations: By averaging over 100 conformers we obtained theoretical cross-sections of 364 Å^2 ($\mathbf{7}\bullet H^+$) and 381 Å^2 ($\mathbf{11}\bullet H^+$), respectively—the monocyclic structure has a slightly larger cross-section, but the difference is small. This difference basically vanishes when averaging over the cross-sections of only the 20 energetically most favored structures: With this method the theoretical cross-section of ($\mathbf{7}\bullet H^+$) remains essentially unchanged (362 Å^2), the cross-section of ($\mathbf{11}\bullet H^+$), however, drops to 363 Å^2 which is now in almost perfect agreement with the experimental value of 362 Å^2.

The finding that the low energy structures of monocyclic ring and catenane have almost identical cross-sections can be rationalized by hydrogen bond interactions that on one hand stabilize the monocyclic

Table 1
Comparison between experimental and theoretical collision cross-sections

Substance	Formula	Experimental collision cross-section (Å^2)	Theoretical collision cross-section[a] (Å^2)
2	$C_{60}H_{64}N_4O_4$–H^+	225	231
3	$C_{59}H_{63}N_5O_4$–H^+	227	230
4	$C_{64}H_{72}N_4O_4$–H^+	244	248
6	$C_{62}H_{68}N_4O_6$–H^+	249	245
7	$C_{120}H_{128}N_8O_8$–H^+	371	364
8	$C_{128}H_{144}N_8O_8$–H^+	397	400
10	$C_{124}H_{136}N_8O_{12}$–H^+	391	385
11	$C_{118}H_{126}N_{10}O_8$–H^+	362	381
12	$C_{177}H_{189}N_{15}O_{12}$–$H^+$	497	499 (541)[b]

[a] Averaged values from projection approximation and exact hard spheres scattering model.
[b] Cross-section calculated for the untwisted ring—this structure can be clearly ruled out on the basis of the experimental cross-section.

ring but on the other hand lead to fairly compact structures; high energy structures on the other hand have significantly larger cross-sections.

This is clearly visible in Fig. 7 which depicts the minimal-energy conformations of octalactam macrocycle **11** (top) and of the *t*-butyl substituted catenane **8** in its protonated forms. The macrocycle forms a significantly self-solvated structure which is stabilized by intramolecular hydrogen bonding between the outer loop and the second half that is folded in. In order to realize such a structure, the conversion of some of the amide bonds into *cis*-amides is required. Since secondary amides usually prefer the *trans*-conformation, it must be assumed that the energy liberated on self-solvation exceeds that necessary for the conformational change of the amide bonds. For the catenane, hydrogen bonding also plays a role for connecting the two macrocycles. The two amide protons of one of the isophthalic acid amide building blocks form a forked hydrogen bond to one of the carbonyl groups of the other macrocycle. For both species, the space filling representation shows the formation of quite densely

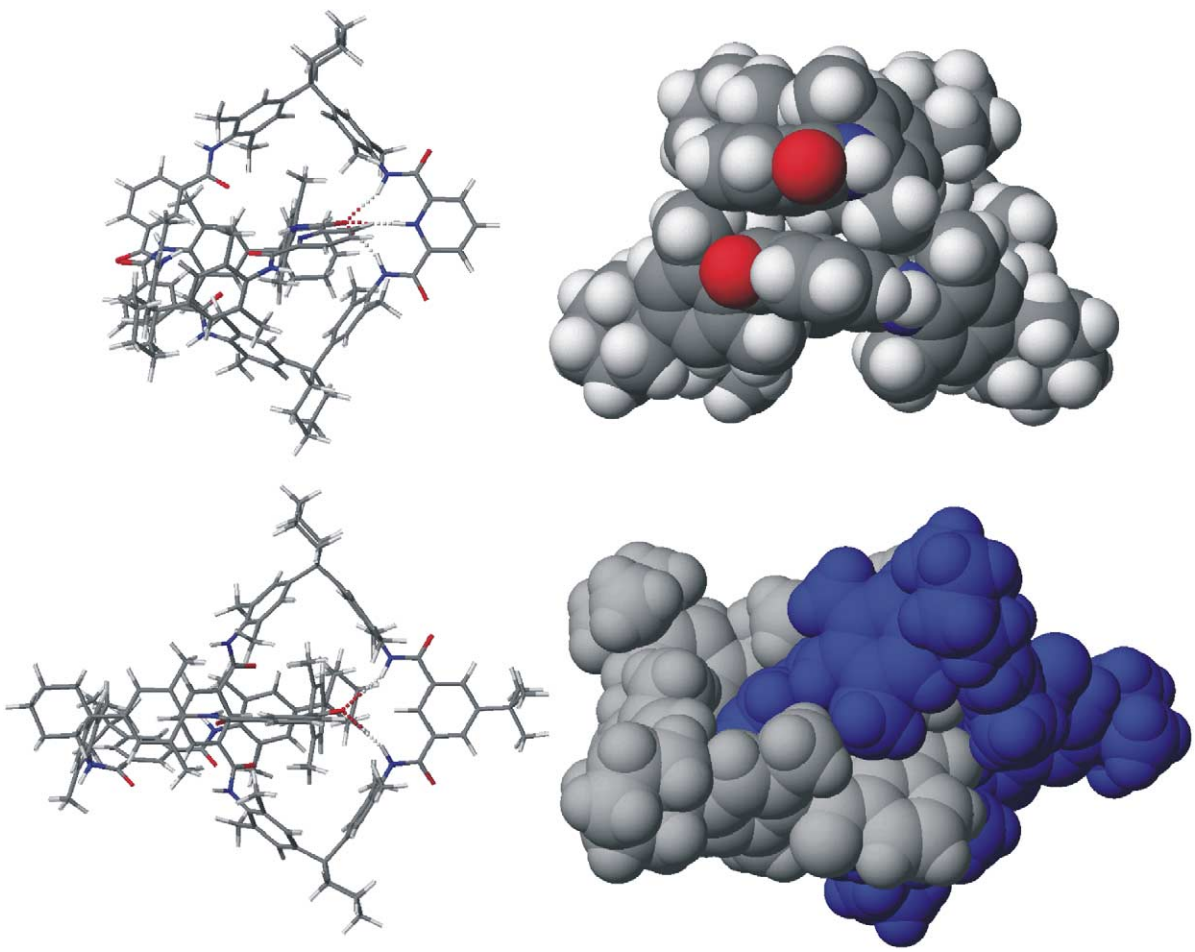

Fig. 7. Top: minimal energy conformation of octalactam macrocycle **11** as stick (left, top view) and space filling (right, side view) representations. Bottom: *t*-butyl substituted catenane **8**. The stick representations show part of the hydrogen bonding patterns, the space filling models show the tight packing of both molecules. Note that the molecular dynamics calculation results in the formation of several secondary *cis*-amides which facilitate self-solvation in the gas phase.

packed, globular-shaped entities, and thus nicely rationalizes why the octalactam macrocycle behaves similar to the catenane in the ion mobility experiments. As a consequence, the ion mobility method is only of limited use for the distinction between the catenanes and the corresponding monocyclic rings—the different fragmentation patterns in the MS/MS spectrum allow a much more unequivocal distinction. It should be noted, however, that ion mobility instruments with higher resolving power exist [31] and that it might be possible to distinguish between catenanes and monocyclic rings with these instruments.

Our experimental cross-section for the trefoil knot **12**•H^+ is 497 $Å^2$, in almost perfect agreement with

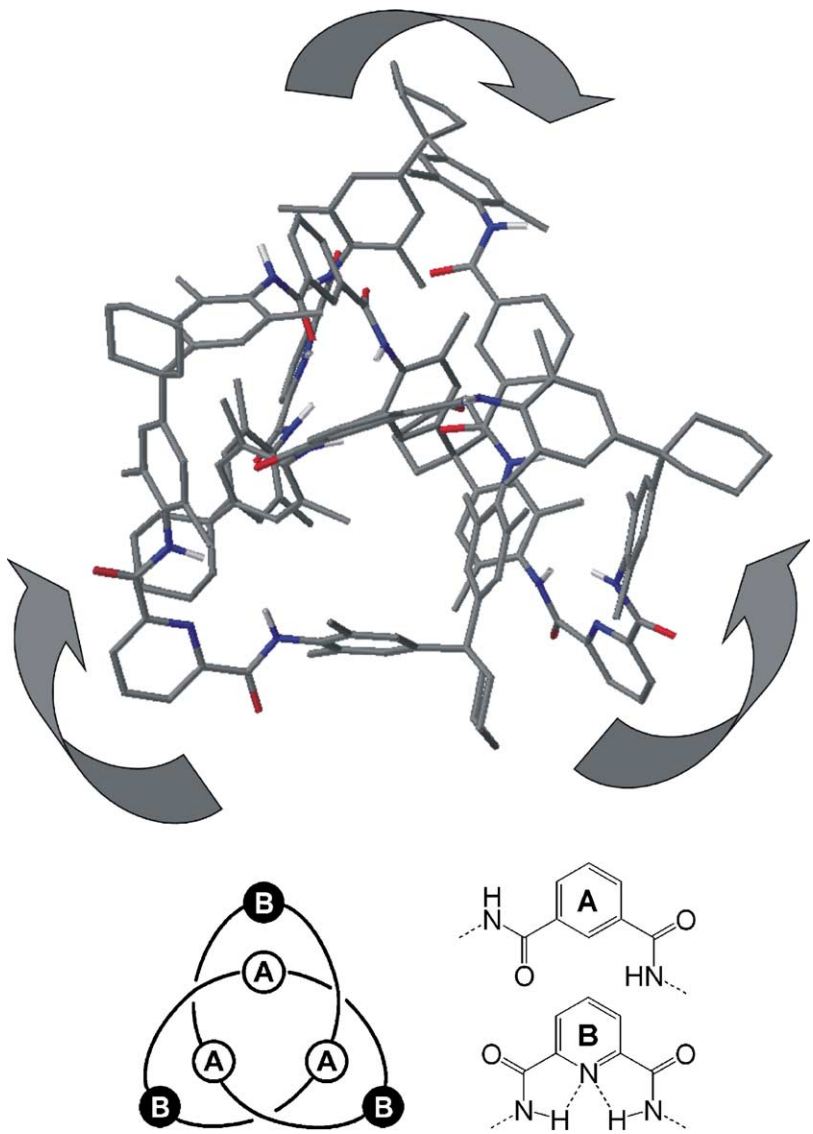

Fig. 8. Minimal-energy conformation of the trefoil knot **12**. For clarity, all carbon-centered hydrogen atoms have been omitted. Arrows indicate the three loops of the knot from back to front. Bottom: schematic drawing and preferred conformations of the isophthalic acid amide and pyridine carboxylic acid amide building blocks. The latter is stabilized by intramolecular hydrogen bonding.

the prediction from the molecular dynamics simulation (499 Å^2). We also calculated the cross-section for the untwisted ring (again 100 conformers averaged) and obtained a value of 541 Å^2. This is almost 10% above the experimental cross-section, and therefore, this untwisted ring structure can be clearly ruled out. In this case, the ion mobility method is superior of the MS/MS method since knots and untwisted monocyclic rings are expected to produce the same fragmentation patterns. Unfortunately, all attempts to synthesize the non-intertwined macrocyclic analogue to the knot failed so far and we are unable to test the fragmentation pattern of this molecule by experiment. It seems nevertheless reasonable to extend the fragmentation patterns found for the other macrocycles to the non-intertwined macrocycle and consequently, the differences of its fragmentation pattern should be minor when compared to that of the knot. Here, the ion mobility method can indeed provide more detailed insight.

The minimal-energy conformation of the protonated knot is shown in Fig. 8. As for **11**, protonation at one of the pyridine nitrogen atoms is more favorable as compared to the protonation of an amide carbonyl group. While the isophthalic acid amide subunits exist in different (in/out)-conformations as indicated in Fig. 8, bottom, the pyridine dicarboxylic acid amide building blocks prefer the conformation indicated in the figure in which both amide protons hydrogen bond intramolecularly to the pyridine nitrogen. This is also the reason, why the three pyridines are located at the knot's periphery. According to simple AM1 calculations, each of these hydrogen bonds possesses a binding energy of somewhat more than 5 kcal/mol, which is in good agreement with recently reported experimental results on the slipping of rotaxane axles out of tetralactam macrocycles bearing either an isophthalic acid amide or a pyridine dicarboxylic acid amide moiety [32].

4. Conclusions

The present study makes a distinction of different topologies of macrocyclic compounds possible and—with easy to perform ESI-MS/MS experiments and collisional activation—provides a simple procedure for the synthetic supramolecular chemist. With this method, it becomes possible to tell apart catenanes and macrocycles, but of course, it is a much greater challenge to distinguish two different topologies of monomacrocyclic compounds, i.e., a knot and a non-intertwined macrocycle. This should however be possible by ion mobility experiments which according to our molecular dynamics results should be different. This approach requires somewhat more sophisticated methodology, but still seems rather straightforward as compared to other methods. Unambiguous characterization of knotted macrocycles so far has been achieved by CD spectroscopy, which relies on a non-routine separation of the two enantiomers of the knot, and on X-ray crystallography which requires that suitable single crystals can be provided [9,10].

Acknowledgements

We are grateful to Prof. Fritz Vögtle, and Prof. Manfred M. Kappes for fruitful discussions. We thank Prof. Konrad Sandhoff for the possibility to use the ESI-MS instrument which was supported by the Deutsche Forschungsgemeinschaft (DFG, "Forschergruppe Keratinozyten—Proliferation und differenzierte Leistung in der Epidermis"). X.-Y. L. thanks the Alexander-von-Humboldt foundation for a postdoctoral fellowship. C.A.S. and P.W. acknowledge financial support from the DFG and the Fonds der Chemischen Industrie.

References

[1] C.A. Hunter, J. Chem. Soc., Chem. Commun. (1991) 749.
[2] C.A. Hunter, J. Am. Chem. Soc. 114 (1992) 5303.
[3] F. Vögtle, T. Dünnwald, T. Schmidt, Acc. Chem. Res. 29 (1996) 451.
[4] G. Schill, Catenanes, Rotaxanes and Knots, Academic Press, New York, 1971.
[5] (a) R. Jäger, F. Vögtle, Angew. Chem. 109 (1997) 966; (b) R. Jäger, F. Vögtle, Angew. Chem. Int. Ed. Engl. 36 (1997) 931.
[6] S.A. Nepogodiev, J.F. Stoddart, Chem. Rev. 98 (1998) 1959.

[7] F.M. Raymo, J.F. Stoddart, Chem. Rev. 99 (1999) 1643.
[8] J.P. Sauvage, C. Dietrich-Buchecker (Eds.), Molecular Catenanes, Rotaxanes, and Knots, Wiley-VCH, Weinheim, 1999.
[9] (a) O. Safarowsky, M. Nieger, R. Fröhlich, F. Vögtle, Angew. Chem. 112 (2000) 1699;
(b) O. Safarowsky, M. Nieger, R. Fröhlich, F. Vögtle, Angew. Chem. Int. Ed. 39 (2000) 1616.
[10] (a) F. Vögtle, A. Hünten, E. Vogel, S. Buschbeck, O. Safarowsky, J. Recker, A. Parham, M. Knott, W.M. Müller, U. Müller, Y. Okamoto, T. Kubota, W. Lindner, E. Francotte, S. Grimme, Angew. Chem. 113 (2001) 2534;
(b) F. Vögtle, A. Hünten, E. Vogel, S. Buschbeck, O. Safarowsky, J. Recker, A. Parham, M. Knott, W.M. Müller, U. Müller, Y. Okamoto, T. Kubota, W. Lindner, E. Francotte, S. Grimme, Angew. Chem. Int. Ed. 40 (2001) 2468.
[11] X.-Y. Li, J. Illigen, M. Nieger, S. Michel, C.A. Schalley, Chem. Eur. J. 9 (2003) 1332.
[12] C.A. Schalley, Int. J. Mass Spectrom. 194 (2000) 11.
[13] C.A. Schalley, Mass Spectrom. Rev. 20 (2001) 253.
[14] E.A. Mason, E.W. McDaniel, Transport Properties of Ions in Gases, Wiley, New York, 1988.
[15] (a) S. Ottens-Hildebrandt, S. Meier, W. Schmidt, F. Vögtle, Angew. Chem. 106 (1994) 1818;
(b) S. Ottens-Hildebrandt, S. Meier, W. Schmidt, F. Vögtle, Angew. Chem. Int. Ed. Engl. 33 (1994) 1767.
[16] (a) F. Vögtle, S. Meier, R. Hoss, Angew. Chem. 104 (1992) 1628;
(b) F. Vögtle, S. Meier, R. Hoss, Angew. Chem. Int. Ed. 31 (1992) 1619.
[17] P.R. Kemper, M.T. Bowers, J. Phys. Chem. 95 (1991) 5134.
[18] G.V. Helden, T. Wyttenbach, M.T. Bowers, Science 267 (1995) 1483.
[19] T. Wyttenbach, G.V. Helden, M.T. Bowers, J. Am. Chem. Soc. 118 (1996) 8355.
[20] K.B. Shelimov, D.E. Clemmer, R.R. Hudgins, M.F. Jarrold, J. Am. Chem. Soc. 119 (1997) 2240.
[21] J. Woenckhaus, Y. Mao, M.F. Jarrold, J. Phys. Chem. B 101 (1997) 847.
[22] R.R. Julian, R. Hodyss, B. Kinnear, M.F. Jarrold, J.L. Beauchamp, J. Phys. Chem. B 106 (2002) 1219.
[23] A.E. Counterman, D.E. Clemmer, J. Phys. Chem. B 105 (2001) 8092.
[24] P. Weis, S. Gilb, P. Gerhardt, M.M. Kappes, Int. J. Mass Spectrom. 216 (2002) 59.
[25] S.J. Weiner, P.A. Kollman, D.A. Case, U.C. Singh, G. Alagona, S. Profeta, P. Weiner, J. Am. Chem. Soc. 106 (1984) 765.
[26] S.J. Weiner, P.A. Kollman, N.T. Nguyen, D.A. Case, J. Comput. Chem. 7 (1987) 230.
[27] D.M. Ferguson, P.A. Kollman, J. Comput. Chem. 12 (1991) 620.
[28] Hyperchem 6, Hypercube Inc., Gainesville, Florida.
[29] G.V. Helden, T. Wyttenbach, M.T. Bowers, Int. J. Mass Spectrom. 146/147 (1995) 349.
[30] A. Shvartsburg, M.F. Jarrold, Chem. Phys. Lett. 261 (1996) 86.
[31] P. Dugourd, R.R. Hudgins, D.E. Clemmer, M.F. Jarrold, Rev. Sci. Instrum. 68 (1997) 1122.
[32] A. Affeld, G.M. Hübner, C. Seel, C.A. Schalley, Eur. J. Org. Chem. (2001) 2877.